all cables described in Table 1 with reproduction factors *less* than 10^{-6}, tidal accelerations must be dissipated by motion imposed at the earth's surface. All cables probably must be provided with mechanisms for such motion.

If necessary, the lower terminus of the initial cable can be founded on a high-altitude structure, such as a tethered balloon, above the influence of significant atmospheric winds. The initial fiber thus has no theoretical gross lower limit of size. A later, generated cable (if not the initial cable) should be founded at the surface, however, and hence the lower limit of its size is determined by drag forces from atmospheric winds.

As examples, we have calculated the lower terminal diameters and resultant total cable masses, assuming that winds at 200 km/hr on a 1-km length of unfaired cable might develop a drag force equal to the cable tension (that is, to produce a 45° departure from the vertical near the lower cable terminus) (Table 1).

For earth conditions the *mechanical* characteristics of conceivable materials give reproduction factors the order of 1/1000 and modest masses for the minimum surface-founded cable. The "theoretical strengths" (Table 1) are greater by at least two orders of magnitude than those attained in present engineering practice and may never be achievable. In this eventuality the required masses will be greater than those tabulated.

The conditions on some other bodies of the solar system appear to be less demanding of materials than the conditions on earth. From the surface of Mars, the Martian satellites, the backside of the earth's moon, some of the Jovian moons and rapidly rotating asteroids, the system probably would be capable of launching large masses to any point in the solar system without excessive demands on materials.

An analysis of the statics of a system extending from a single rotating body follows.

The mechanics of such a system installed on an isolated rotating body can be treated in terms of the following parameters: r = radial distance from the center of the body (height); $A(r)$ = cross-sectional area of cable at height r; $T(r)$ = tension in cable at height r; Y = yield stress of cable; ρ = density of cable; m = mass attached to top of cable; M = mass of cable; a = radius of planet; ω = angular velocity of planet; g = surface gravity of planet; $\epsilon = a\omega^2/g$ = ellipticity of planet; $\lambda = (g\ a^2\ \omega^{-2})^{1/3}$ = radius of stationary orbit; $\gamma = \rho\ Y^{-1}\ (g\ a^2\ \omega)^{2/3}$; $\psi(s) = (1 - s)^2\ [(\frac{1}{2}) + (1/s)]$, where s is any functional variable. For the earth, $\lambda = 4.22 \times 10^9$ cm and $\gamma = \rho\ Y^{-1}\ 9.45 \times 10^{10}$, $\gamma\ \psi\ (a/\lambda) = \rho\ Y^{-1}\ 4.85 \times 10^{11}$ in *cgs* units.

If the cable is stressed to its yield strength everywhere, then

$$A(r) = A(\lambda)e^{-\gamma\psi(r/\lambda)}$$

In particular, $A(\lambda)$ is the maximum value of $A(r)$, and $\ln\ [A(\lambda)/A(a)] =$

$$\frac{\rho}{Y} ga\left(1-\frac{a}{\lambda}\right)^2 \left(1+\frac{a}{2\lambda}\right)$$

For the earth $a/\lambda = 0.151$; then

$$A(\lambda)/A(a) \approx e^{(\rho/Y)ga}$$

Note here that the thickening of the cable from the bottom at $r = a$ to the thickest point at $r = \lambda$ is approximately independent of ω.

The ratio of the mass of the apparatus, $(M + m)$, to the mass of the load it can lift, $T(a)/g$, is

$$\frac{g(M+m)}{T(a)} = \epsilon^{-2/3}\, e^{\gamma\psi(a/\lambda)} \times \left[\frac{\lambda R^2}{R^3-\lambda^3} e^{-\gamma\psi(R/\lambda)} + \gamma \int_{a/\lambda}^{R/\lambda} e^{-\gamma\psi(\sigma)} d_\sigma\right]$$

For a fixed total mass $(M + m)$, this ratio is minimized [and the load $T(a)/g$ maximized] by taking $R = \infty$, $m = 0$. The difference between $R = 3\ \lambda$ and $R = \infty$ is negligible for realistic values of γ. When $R = \infty$ and $m = 0$,

$$gM/T(a) = \gamma\epsilon^{-2/3}e^{\gamma\psi(a/\lambda)} \int_{a/\lambda}^{\infty} e^{-\gamma\psi(s)} ds$$

Then the total mass of material to constitute the inital cable would be:

$$M = \lambda\rho A(a)e^{\gamma\psi(a/\lambda)} \int_{a/\lambda}^{\infty} e^{-\gamma\psi(s)} ds$$

The minimum acceptable value of $A(a)$ is set by practical considerations of wind drag and anchoring force in the cable. (The anchoring force is also, of course, the maximum weight, including acceleration, of a vehicle that climbs the cable.)

The installation from a revolving *and* rotating body is ordinarily subject to two choices of the *modus operandi*. The analysis is much more complex.

JOHN D. ISAACS
Scripps Institute of Oceanography, University of California, La Jolla
ALLYN C. VINE
Woods Hole Oceanographic Institute, Woods Hole, Massachusetts
HUGH BRADNER
GEORGE E. BACHUS
Scripps Institute of Oceanography

References and Notes

1. The device would be continuously tapered with its maximum diameter at the radius of the synchronous orbit.
2. We have not considered conditions in the ionosphere and in space that might have deleterious effects upon any material employed; we have not estimated the probability of collision with meteoroids or man-made satellites; and we have examined only the obvious linear problems of stability. We are quite aware that the engineering problems inherent in this system could be answered only by a program commensurate with some of the large contemporary projects.
3. A. H. Cottrell, *The Mechanical Properties of Matter* (Wiley, New York, 1964), p. 235.
4. A. Kelly, *Sci. Amer.* **212**, 28 (1965).
5. R. Bacon, in *Growth and Perfection of Crystals*, R. H. Doremus, B. W. Roberts, D. Turnbull, Eds. (Wiley, New York, 1958).
6. American Institute of Physics Handbook (New York, 1963), sec. 2, p. 52.

26 November 1965

Ammonium Micas: Possible Sources of Atmospheric Ammonia and Nitrogen

Abstract. *Ammonium muscovite,* $NH_4Al_2AlSi_3O_{10}(OH)_2$, *and ammonium phlogopite,* $NH_4Mg_3AlSi_3O_{10}(OH)_2$, *have been synthesized hydrothermally at gas pressures of 2 kilobars and temperatures between 550° and 730°C. Both micas are stable only in environments of high ammonia fugacity. Ammonia or nitrogen, or both, are released by thermal decomposition, cation exchange, or oxidation. The ammonia : nitrogen ratio in the gas depends primarily on the hydrogen fugacity and the temperature of the environment. Calculations show that, even in a predifferentiated Earth, nitrogen may have predominated. The total amount of nitrogen present on the surface of Earth could be accounted for by the decomposition of a layer of ammonium muscovite 170 meters thick.*

The origin and the composition of the terrestrial primitive atmosphere have recently been extensively discussed (*1*). Considerable evidence supports the theory that the atmosphere accumulated from degassing of Earth throughout its geologic history. Common constituents during the earliest periods are assumed to be CH_4, NH_3, and H_2O. The primary sources of the ammonia, and hence of the nitrogen in today's atmosphere, were presumably either ammonium silicates or metal nitrides.

The average nitrogen content of igneous and metamorphic rocks and minerals is low (*2*), with micas containing in general the largest amounts. Silicates from unusual environments may be greatly enriched in ammonia.

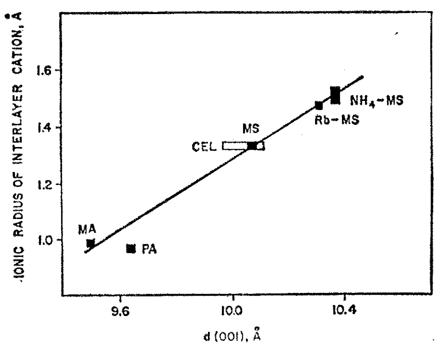

Fig. 1. Spacing of (001) for 1M polymorphs of a number of synthetic dioctahedral micas (*8*) as a function of the ionic radius of the interlayer cation; *d*(001) for celadonite varies with f_{O_2}. The radius of NH_4^+ in silicates is uncertain; an average value is plotted. *MA*, margarite; *PA*, paragonite; *MS*, muscovite; *CEL*, celadonite; *Rb-MS*, rubidium muscovite; *NH_4-MS*, ammonium muscovite.

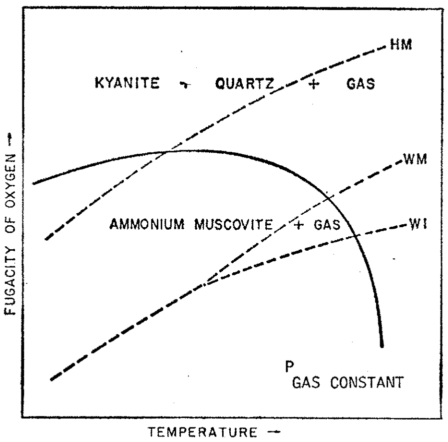

Fig. 2. Schematic representation of the stability field of ammonium muscovite as a function of oxygen fugacity and temperature at a constant gas pressure. *HM*, *WM*, and *WI* are the f_{O_2}-T curves for the assemblages hematite + magnetite + gas, wüstite + magnetite + gas, and wüstite + iron + gas; they are added for reference. For exact locations see (*9*).

The feldspar buddingtonite contains 8.3 percent by weight of $(NH_4)_2O$ (*3*). Vedder (*4*) has shown that $(NH_4)^+$ can proxy for K^+ in the interlayer sites of micas. Buddingtonite has been synthesized by Barker (*5*), and synthesis of ammonium muscovites has been reported by Gruner and by Barrer and Denny (*6*).

In an effort to test the mechanisms by which ammonia or nitrogen can be released from ammonium silicates, we have synthesized an ammonium muscovite and an ammonium phlogopite at gas pressures of 2 kb (Table 1). The ammonium muscovite grows readily in a vapor rich in NH_3 at temperatures up to 670°C; this temperature is comparable to the upper stability limit of muscovite at the same pressure (*7*). The ammonia fugacity in the vapor phase is unknown but is probably of the order of several hundred bars. If the gas phase initially contains only H_2O, no ammonium muscovite forms from the mixture, and the synthetic ammonium muscovite decomposes to quartz plus an alumino-silicate. Similarly, the ammonium phlogopite can be synthesized readily in the presence of a vapor rich in NH_3, but is replaced in the presence of a water-rich vapor by talc plus forsterite plus spinel at high temperatures, and by talc plus chlorite at lower temperatures. For quantitative study of the stability relations of these ammonium silicates, it will be necessary to control the fugacities of H_2O and NH_3 simultaneously; such a method is now being developed.

X-ray properties of the two ammonium micas are summarized in Tables 2 and 3. Figure 1 shows the effect of the size of the interlayer cation on *d*(001) for a number of dioctahedral micas (*8*); the ammonium muscovite is the mica with the largest basal spacing.

Ammonia may be released from ammonium silicates by one of three types of reactions: thermal decomposition, cation exchange, and oxidation. For ammonium muscovite the three reactions would be

$$\underset{\text{ammonium muscovite}}{2\,\mathrm{NH_4Al_2AlSi_3O_{10}(OH)_2}} \rightleftharpoons \underset{\text{kyanite}}{3\,\mathrm{Al_2SiO_5}} + \underset{\text{quartz}}{3\,\mathrm{SiO_2}} + 2\,\mathrm{NH_3} + 3\,\mathrm{H_2O} \quad (1)$$

$$\underset{\text{ammonium muscovite}}{\mathrm{NH_4Al_2AlSi_3O_{10}(OH)_2}} + \mathrm{K^+} \rightleftharpoons \underset{\text{muscovite}}{\mathrm{K\ Al_2AlSi_3O_{10}(OH)_2}} + \mathrm{NH_4^+} \quad (2)$$

$$\underset{\text{ammonium muscovite}}{2\,\mathrm{NH_4Al_2AlSi_3O_{10}(OH)_2}} + \frac{3}{2}\mathrm{O_2} \rightleftharpoons \underset{\text{kyanite}}{3\,\mathrm{Al_2SiO_5}} + \underset{\text{quartz}}{3\,\mathrm{SiO_2}} + \mathrm{N_2} + 6\,\mathrm{H_2O} \quad (3)$$

Reaction 1 proceeds within a temperature range common for dioctahedral micas, while Reaction 2 can move to the right presumably at much lower temperatures in environments of high $a_{K^+} : a_{NH_4}$ ratios. Reaction 3 is obtained from 1 by adding Reactions 4 and 5:

$$2\mathrm{NH_3} \rightleftharpoons \mathrm{N_2} + 3\,\mathrm{H_2} \quad (4)$$

$$3\mathrm{H_2} + \frac{3}{2}\mathrm{O_2} \rightleftharpoons 3\,\mathrm{H_2O} \quad (5)$$

Judged by oxidation reactions of other micas (*9*), Reaction 3 should proceed to the right at temperatures as low as 200° to 300°C for reasonable values of the oxygen fugacity.

Figure 2 shows the probable shape of the stability field of ammonium muscovite for a given gas pressure as a function of oxygen fugacity and temperature; the dashed curves are for iron oxide assemblages and are added for

Table 1. Results of experiments in synthesis of ammonium muscovite and ammonium phlogopite at gas pressures of 2 kb. Synthesis was carried out in sealed gold tubes containing about 30 mg of solids and 15 mg of liquid—either distilled water or 15-percent NH_4OH. Abbreviations: NH_4-MS, synthetic ammonium muscovite; NH_4-Ph, synthetic ammonium phlogopite; Ms-mix, a mixture of NH_4HCO_3 + γ-Al_2O_3 + SiO_2 of ammonium muscovite composition; Ph-mix, a mixture of NH_4HCO_3 + MgO + γ-Al_2O_3 + SiO_2 of ammonium phlogopite composition; x, an unknown phase with reflections at 3.48, 2.38, and 1.74 Å.

Starting material	Temp. (°C)	Time (days)	Phases produced
		Ammonium muscovite	
NH_4-Ms + NH_3	752	7	Mullite + quartz + x
NH_4-Ms + H_2O	745	6	Mullite + quartz
NH_4-Ms + NH_3	730	1	Mullite + quartz + andalusite + x
NH_4-Ms + NH_3	701	8	Mullite + quartz
NH_4-Ms + NH_3	670	16	NH_4-Ms
NH_4-Ms + NH_3	640	5	NH_4-Ms
NH_4-Ms + H_2O	640	5	Mullite + andalusite + quartz
NH_4-Ms + NH_3	600	10	NH_4-Ms
Ms-mix + H_2O	555	10	NH_4-Ms + quartz
Kaolinite + NH_3	550	5	NH_4-Ms
		Ammonium phlogopite	
Ph-mix + H_2O	745	6	Talc + forsterite + spinel
Ph-mix + NH_3	730	1	NH_4-Ph
NH_4-Ph + NH_3	600	8	NH_4-Ph
NH_4-Ph + H_2O	600	8	Talc + 7-Å chlorite
Ph-mix + H_2O	600	2	Talc + 7-Å chlorite
Ph-mix + H_2O	550	10	NH_4-Ph

Table 2. X-ray powder data for ammonium muscovite and ammonium phlogopite. All reflections were measured against an internal silicon standard (ammonium phlogopite) and an internal quartz standard (ammonium muscovite) by use of a Norelco diffractometer. Values used for the standards were: $a = 5.4306$ Å for silicon at 18°C; $a = 4.9131$ Å and $c = 5.4046$ Å, for quartz at 18°C.

Cu$K\alpha$ 2θ, obs.	d(Å) Observed	d(Å) Calculated	I:Io	(hkl)
		Ammonium muscovite		
8.5	10.4	10.334	100	001
17.175*	5.163	5.167	50	002
19.738*	4.498	4.501	50	020
20.344*	4.365	4.366	25	110
21.5	4.13	4.127	5	021
24.064*	3.698	3.698	30	$\bar{1}12$
25.870*	3.444	3.445	50	003
28.640*	3.117	3.117	20	112
30.0	2.98	2.982	3	$\bar{1}13$
32.733*	2.736	2.735	5	023
34.873*	2.573	2.572	35	$\bar{1}31$
36.5	2.46	2.454	15	131
37.279	2.412	2.421 2.412	15	$\bar{1}14$ $\bar{1}32$
37.9	2.37	2.378	3	201
43.793*	2.067	2.068	15	005
53.9	1.70	1.703 1.700 1.698 1.697	10	$\bar{2}41$ $\bar{1}35$ 150 044
54.8	1.67	1.675 1.671	4	310 $\bar{2}42$
61.704	1.503	1.504 1.500	15	$\bar{3}31$ 060
		Ammonium phlogopite		
8.6	10.3	10.293	100	001
17.275*	5.133	5.147	30	002
19.298*	4.599	4.612	30	020
19.500*	4.552	4.552	30	110
20.135*	4.410	4.410	2	$\bar{1}11$
24.120*	3.690	3.690	5	$\bar{1}12$
25.970*	3.431	3.431	80	003
28.010*	3.185	3.185	7	112
30.2	2.96	2.957	3	$\bar{1}13$
32.4	2.76	2.753	2	023
34.165	2.624	2.622 2.617	45	$\bar{1}31$ 200
34.888	2.572	2.573 2.565	10	004 113
35.705	2.515	2.516 2.511	15	131 $\bar{2}02$
36.719	2.447	2.444 2.440	60	$\bar{1}32$ 201
41.210	2.191	2.191 2.188	20	$\bar{1}33$ 202
43.966*	2.059	2.059	20	005
45.0	2.01	2.016 2.013	10	133 $\bar{2}04$
54.0	1.70	1.698 1.698 1.697	5	$\bar{2}42$ $\bar{1}35$ 204
60.180*	1.538	1.537	15	060

* Reflection used in the least-squares refinement.

Table 3. Cell dimensions of ammonium and potassium micas; determined from the powder data of Table 2 with a 3-cycle least-squares refinement, by use of Burnham's computer program (*11*); data for phlogopite and muscovite from (*7*).

Phase	a(Å)	b(Å)	c(Å)	β	Cell volume (Å^3)	Calculated density (g cm^{-3})
Phlogopite	5.314	9.204	10.314	99°54′		
Ammonium phlogopite	5.311 ± 0.008	9.224 ± 0.004	10.443 ± 0.007	99°42′	504.19	2.61
Muscovite	5.208	8.995	10.275	101°35′		
Ammonium muscovite	5.217 ± 0.003	9.001 ± 0.003	10.540 ± 0.002	101°22′	485.33	2.58

reference (*9*). At low values of f_{O_2}, Reaction 1 predominates and the maximum stability temperature is comparable to that of muscovite. With increasing f_{O_2}, Reaction 3 becomes gradually dominant and the decomposition temperature is reduced. The composition of the gas phase changes drastically from low to high values of f_{O_2} and can be calculated from the equilibrium constants defined by:

$$(K_1)_{P,T} = (f^3{}_{H_2} \times f_{N_2})/f^2{}_{NH_3} \quad \text{(from Reaction 4)}$$

$$(K_2)_{P,T} = (f^2{}_{N_2} \times f^6{}_{H_2O})/(f^4{}_{NH_3} \times f^3{}_{O_2})$$

(from Reaction 4 plus 5)

This dependence of the equilibrium constants on the gas composition is probably the reason why Barker (*5*), though he was able to synthesize an almost potassium-free buddingtonite, could not preserve it for more than 3 days under the conditions of synthesis.

Of most interest with respect to degassing of ammonium silicates is the value of the ammonia : nitrogen ratio in the gas phase in equilibrium with such silicates; this is determined by pressure, temperature, and the hydrogen fugacity, $f_{H_2}(K_1)$. One may evaluate these parameters for probable conditions at which degassing took place. Figure 3 shows the ratio $f^2{}_{NH_3} : f_{N_2}$ as a function of the hydrogen fugacity and temperature, whereby the value of 1 may be taken as the dividing line between a gas phase rich in ammonia and one rich in $N_2 + H_2$.

French (*10*) has calculated the hydrogen partial pressures for the assemblage fayalite plus quartz plus iron plus graphite from thermochemical data. This assemblage can be taken to represent primitive crustal material. From the hydrogen fugacities of this assemblage at a number of gas pressures (Fig. 3) it is evident that degassing under these conditions would lead to dominance of nitrogen over ammonia even at reasonably high temperatures and pressures; that is, Reaction 3 is more important than Reaction 1.

Hydrogen fugacities can be much higher if graphite is absent. A gas in the system O—H for instance, in equilibrium with the fayalite-quartz-iron assemblage, consists essentially of pure hydrogen (*9*). In such an environment, ammonia would greatly dominate nitrogen; thus gassing from a predifferentiated Earth *may* have led to predominance of ammonia, but only if iron was present and graphite was absent. Beginning with the separation into crust and mantle, if not much earlier, the equilibrium shifted away from ammonia toward nitrogen, and the already present ammonia was oxidized in part perhaps with oxygen supplied by the solids present.

The total amount of nitrogen present at Earth's surface has been estimated at about 4 × 10^{15} tons (*12*). This amount

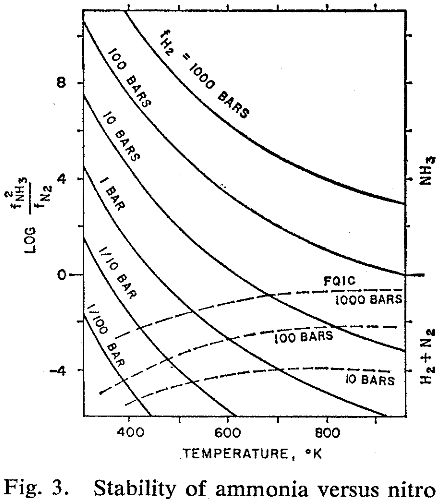

Fig. 3. Stability of ammonia versus nitrogen + hydrogen as a function of hydrogen fugacity and temperature (solid curves), as calculated from thermodynamic data. The hydrogen pressures of the assemblage fayalite + quartz + iron + graphite + gas for total pressures of 1000, 100, and 10 bars, as calculated by French (*10*), were used to plot the dashed curves (*FQIC*).

includes both the nitrogen now in the atmosphere and that present in living matter and in sediments; it is probably a good measure of the total amount of nitrogen accumulated by degassing. Such an amount would be released by decomposition of 2×10^{17} tons of ammonium muscovite—a layer 170 m thick at Earth's surface. If one used ammonium feldspar as a basis for these calculations, the layer would be 70 m thick. This is clearly a trivial amount of matter compared with the total mass of Earth. The average natural muscovite contains 60×10^{-6} g of N_2 per gram, or 0.32 percent ammonium muscovite (*2*). Thus a layer of this average muscovite about 50 km thick would have to be degassed to yield the nitrogen present on Earth's surface today. There is no guarantee, however, that this average muscovite has not already lost most of its ammonia.

HANS P. EUGSTER
JAMES MUNOZ

Department of Geology,
Johns Hopkins University,
Baltimore, Maryland

References and Notes

1. W. W. Rubey, *Bull. Geol. Soc. Amer.* **62**, 1111 (1951); H. D. Holland, in *Petrologic Studies: A Volume to Honor A. F. Buddington* (Geol. Soc. Amer., New York, 1962); *Proc. Nat. Acad. Sci. U.S.* **53**, 1173 (1965).
2. F. Wlotzka, *Geochim. Cosmochim. Acta* **24**, 106 (1961).
3. R. C. Erd, D. E. White, J. J. Fahey, D. E. Lee, *Amer. Mineralogist* **49**, 831 (1964).
4. W. Vedder, *Geochim. Cosmochim. Acta* **29**, 221 (1964).
5. D. S. Barker, *Amer. Mineralogist* **49**, 851 (1964).
6. E. Gruner, *ibid.* **24**, 428 (1939); R. M. Barrer and P. J. Denny, *J. Chem. Soc.* **1961**, 971 (1961).
7. H. S. Yoder and H. P. Eugster, *Geochim. Cosmochim. Acta* **8**, 225 (1955).
8. The values for *d*(001) of synthetic micas are from the following sources: margarite, H. P. Eugster, unpublished data; paragonite, ——— and H. S. Yoder, *Geol. Soc. Amer. Bull.* **65**, 1248 (1954); muscovite, (*7*); celadonite, W. S. Wise and H. P. Eugster, *Amer. Mineralogist* **49**, 1031 (1964); Rb-muscovite, H. P. Eugster and L. Meckel, unpublished data.
9. H. P. Eugster and D. R. Wones, *J. Petrol.* **3**, 82 (1962).
10. B. M. French, in *NASA Report X-641-65-324* (1965).
11. C. W. Burnham, in *Carnegie Inst. Wash. Year Book 1961* (1962), p. 132.
12. For the most recent estimates see K. H. Wedepohl, *Fortschr. Geol. Rheinland Westfalen* **10**, 129 (1963).
13. Supported by a grant from the Petroleum Research Fund of the American Chemical Society. We thank B. M. French for permission to use his data on gas compositions in the system C—H—O.

4 November 1965

■

Thunderstorm Electrification of Hail and Graupel by Polar Dribble

Abstract. *Hail and graupel falling through rain collect water that selectively dribbles upward from the upper surface of a hailstone. When the hailstones are polarized by nearly vertical electrostatic field these vertically discharged water drops carry away free charge of the same sign as that induced on the upper surfaces. The hail thereby accumulates an equilibrium charge of opposite sign, corresponding to the charges induced on the bottom surfaces. The equilibrium charges are large enough to be important in thunderstorms.*

Large electrification effects are usually observed in thunderstorms whenever hail or graupel is present. An induction process that transfers large free electrical charges to such hailstones or graupel is considered below. The process is somewhat related to the Elster and Geitel mechanism that considers the charges carried away by impinging cloud droplets reflected from raindrops (*1*).

Assume that an insulated but conducting spherical shell is exposed to an impressed electric field E_0 as shown in Fig. 1. This field polarizes the sphere to establish on its surface a field E, in electrostatic units, of magnitude

$$E = 4\pi\sigma = 3\,E_0 \cos\varphi \qquad (1)$$

where φ is the angle with respect to the axis of polarization and σ is the free static charge per unit area.

Suppose now that the shell is partly filled with water that is allowed to dribble out a small hole at the pole, P, and fall away. Each drop will carry away charge proportional to the electric field at the point of droplet detachment. In this way, free charge is progressively transferred away from the sphere, which simultaneously builds up an opposite free charge on the shell proper. The transfer of charges continues until the electric field at the point of droplet detachment is reduced to zero. Laboratory tests clearly show that when this equilibrium state is reached, the sphere is charged to the value given by Eq. 2.

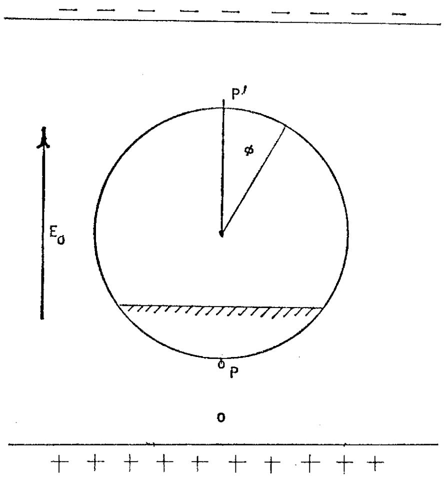

Fig. 1. Diagram of experimental arrangement.

Consider an interesting case where the impressed electric field is vertically upward, as shown in Fig. 1, and the drops are detached at the lower pole, P. The charges induced at the lower pole are negative, so that the water drops carry away negative charges, leaving the shell more positive. The positive charge will increase as drops are lost until the electric field at the bottom pole approaches zero. Since by Eq. 1 the field at the bottom pole was initially inward with a magnitude $3\,E_0$, it can be neutralized only by the accumulation of charge on the sphere sufficient to give an outward field of $3\,E_0$ at the bottom pole. Thus, the equilibrium charge on the shell of radius a is (in electrostatic units)

$$Q = 3\,E_0a^2 \qquad (2)$$

It is important to notice that if the drops were detached from the top pole, P', by some special mechanism, then the accumulated free charge would be of opposite sign. This is actually what happens when hail or graupel falls through rain clouds. The weakly charged rain swept up by the falling hail wets and accumulates on the surface of the hail or graupel but then dribbles *upward* from the rapidly falling hailstones. This process has been well demonstrated (see *2*, fig. 13). Accordingly, if one adopts the outward-drawn normal as the positive direction for E_0, the free charge, Q, accumulated on falling hail and graupel particles approximates (in electrostatic units)

$$Q = -3\,E_0a^2 \qquad (3)$$

Because of the large size of hailstones and the large measured electric fields usually encountered near the